Time-domain measurement of optical activity by an ultrastable common-path interferometer

Preda, Fabrizio ; Perri, Antonio ; Réhault, Julien ; Dutta, Biplab ; Helbing, Jan ; Cerullo, Giulio ; Polli, Dario

Abstract: We introduce a novel configuration for the broadband measurement of the optical activity of molecules, combining time-domain detection with heterodyne amplification. A birefringent common-path polarization-division interferometer creates two phase-locked replicas of the input light with orthogonal polarization. The more intense replica interacts with the sample, producing a chiral free-induction decay field, which interferes with the other replica, acting as a time-delayed phase-coherent local oscillator. By recording the delay-dependent interferogram, we obtain by a Fourier transform both the circular dichroism and circular birefringence spectra. Our compact, low-cost setup accepts ultrashort light pulses, making it suitable for measurement of transient optical activity.

DOI: https://doi.org/10.1364/ol.43.001882

ORIGINAL ARTICLE

Time-domain measurement of optical activity by an ultra-stable common-path interferometer

Fabrizio Preda[1], Antonio Perri[1], Julien Réhault[2], Biplab Dutta[3,4], Jan Helbing[3], Giulio Cerullo[1,5] and Dario Polli[1,6*]

We introduce a simple configuration for the broadband measurement of the optical activity of molecules, which combines time-domain detection with heterodyne amplification. A birefringent common-path polarization-division interferometer creates two intrinsically phase-locked replicas of the input light with orthogonal polarization. The more intense replica interacts with the sample, producing a chiral free-induction decay field interfering with the other replica, which acts as a time-delayed phase-coherent local oscillator and amplifies the chiral field. By recording the interferogram as a function of the relative delay on a single detector, we simultaneously obtain by a Fourier transform both the circular dichroism and circular birefringence spectra. Our configuration is compact, low-cost and, with respect to conventional spectropolarimeters, it dispenses with monochromator, photo-elastic modulator and lock-in detection. Furthermore, it accepts ultrashort pulses, making it suitable for time-resolved measurements of optical activity on the femtosecond timescale.

Keywords: chirality, optical activity, interferometry, Fourier transform spectroscopy

[1] Dipartimento di Fisica, Politecnico di Milano, Piazza Leonardo da Vinci 32, I-20133 Milano, Italy

[2] Institute of Applied Physics, University of Bern, Sidlerstrasse 5, 3012 Bern, Switzerland

[3] University of Zurich, Department of Chemistry, Winterthurerstrasse 190, 8057 Zurich, Switzerland

[4] present address: AMOLF, Science Park 104, 1098 XG, Amsterdam, The Netherlands

[5] IFN-CNR, Piazza Leonardo da Vinci 32, 20133 Milano, Italy

[6] Center for Nano Science and Technology @PoliMi, Istituto Italiano di Tecnologia, Via Giovanni Pascoli 70/3, 20133 Milano, Italy

[*] Correspondence: D Polli, E-mail: dario.polli@polimi.it

INTRODUCTION

The chirality of molecules is of paramount importance in biology and chemistry, as it has a strong influence on biological functions, such as enantioselective catalytic reactions or binding of drugs with the target biomolecules[1]. For this reason, the distinction of a chiral molecule from its mirror image and the identification of their handedness are extremely important for the chemical, pharmaceutic and food industries. Interaction of chiral molecules with light gives rise to optical activity (OA)[2,3], which manifests itself in circular dichroism (CD) and circular birefringence (CB), i.e. difference in absorbance and refraction, respectively, between left (LCP) and right (RCP) circularly polarized light. OA also arises from the chiral arrangement of chromophores in biopolymers, such as proteins and nucleic acids. Ultraviolet (UV) CD spectroscopy is thus a powerful tool for structural studies and can distinguish between α-helix, β-sheet, and random coil conformations of proteins, determine their secondary structure content, as well as monitor their stability and study their folding processes[4,5]. The concept of chirality has also been recently extended to plasmonic systems, exploiting the handedness either of single nanostructures or of their spatial arrangement,[6] showing the potential to increase detection sensitivity thanks to the enhanced light-matter interaction.

When a linearly polarized light field impinges on an achiral medium, it drives a time-varying material polarization which in turn radiates a light field, the achiral free induction decay (AFID); interference of the AFID with the input field gives rise to linear absorption/refraction. A chiral medium, conversely, radiates a small light field with perpendicular polarization, known as chiral FID (CFID), which changes the polarization state of the output light, turning it from linear to elliptical[7,8]. As the CFID field is very weak, CD/CB are orders of magnitude smaller than the corresponding achiral absorption/refraction, making their experimental measurement challenging. Standard CD spectrometers (also known as spectropolarimeters) rely on fast polarization modulation and synchronous detection to extract the differential absorption of the RCP and LCP light by a chiral sample. In the visible/UV range, spectropolarimeters work in the frequency domain: a photo-elastic modulator (PEM) switches the polarization of a monochromatized light beam between RCP and LCP at tens of kHz frequency, and the tiny absorbance difference is measured by a lock-in amplifier. By scanning the excitation light wavelength with a monochromator, it is possible to record a CD spectrum with very high sensitivity in a typical measurement time of the order of minutes. In the mid-IR, vibrational CD (VCD) is typically measured in the time domain by Fourier-Transform (FT) IR spectrometers, in which the polarization of the output of an amplitude division interferometer (such as a Michelson) is modulated by a PEM. When an additional polarizer is added between sample and detector CB spectra can also be recorded[9]. Although well established and commercially available, these classical approaches to CD/VCD require a rather complex, bulky and expensive instrumentation.

Alternative configurations for measuring CD use a polarization-division interferometer (PDI), that is a modified amplitude-division interferometer in which the light in the two arms is linearly polarized in perpendicular directions[10]. Ragunathan et al.[11] and Polavarapu et al.[12] used a modified Michelson interferometer to record VCD spectra in the time domain. As the optical path length difference between the arms is varied, the polarization of the interferometer output quickly changes between LCP and RCP, whereas the overall light intensity is constant, because perpendicularly polarized components do not

interfere. Only in the presence of a chiral sample can an interferogram be recorded, and the CD (or linear dichroism) spectrum can be retrieved by a FT. Rhee et al.[13,14] used a free-space Mach-Zehnder interferometer and employed spectral interferometry the frequency domain[15]. The interferometer was adjusted to generate an intense replica with vertical (V) polarization and a weaker one with horizontal (H) polarization. Instead of scanning the interferometer delay τ and recording the signal in the time domain, τ was fixed and the light transmitted by the sample was dispersed on a spectrometer after passing through a linear polarizer (analyzer) with very high extinction ratio and aligned along the H direction. In this configuration, the CFID field with H polarization, generated by the interaction of the V polarization with the chiral sample, interferes with the H polarized replica, acting as a local oscillator (LO). This yields, via a Kramers-Kronig transform, the complex chiral signal $S_H(\omega,\tau)$. A second measurement with analyzer aligned along the V direction, produces an achiral reference signal $S_V(\omega,\tau)$. The CD and CB spectra can then be calculated as[16]: $\frac{S_H(\omega,\tau)}{S_V(\omega,\tau)} = CB(\omega) + iCD(\omega)$. The main limitation of interferometric approaches is the required high path-length stability between the two arms of the interferometer, since any mechanical vibration by a fraction of wavelength would spoil the measurement. This stability is more easily achieved for VCD which works at long wavelengths in the mid-IR (λ>3 μm); at shorter wavelengths, active stabilization of the interferometer or simultaneous single-shot detection of $S_H(\omega,\tau)$ and $S_V(\omega,\tau)$. using a dual-channel spectrometer[17,18] are required.

In this work, we introduce a novel and remarkably simple time-domain approach to electronic OA measurements in the visible/near-IR range. Our method uses an intrinsically phase-stable birefringent common-path interferometer (CPI) to generate two phase-locked perpendicularly polarized replicas of the broadband input light without any active stabilization or delay tracking. The replica with weaker amplitude acts as LO, phase-locked to the CFID field generated by the other replica. By scanning the delay between replicas and recording the interferogram between LO and CFID with a single detector, one can simultaneously obtain with an FT both the CD and CB spectra. We demonstrate operation with incoherent light and with ultrashort laser pulses, illustrating the potential of a compact, robust and low-cost alternative to standard spectropolarimeters. Importantly, our CPI accepts broadband ultrashort light pulses, thus paving the way to ultrafast detection of OA on the femtosecond timescale.

MATERIALS AND METHODS

Measurement principle

Figure 1 shows the conceptual scheme of our spectropolarimeter. A first polarizer (P_1) creates an input field linearly polarized at an angle γ with respect to the V direction. This field crosses the CPI, which splits it into two replicas with V and H polarization and relative delay τ. As OA is a linear optical property, we can apply the superposition principle and decompose the broadband illumination light into monochromatic waves with angular frequency ω and amplitude $E_0(\omega)$. For each of these waves, the Jones vector[19] that describes the electric field after the CPI is:

$$E_{in}(\omega,\tau) = E_0(\omega)\begin{pmatrix}\sin\gamma \\ \cos\gamma\cdot e^{i\varphi}\end{pmatrix} \qquad (1)$$

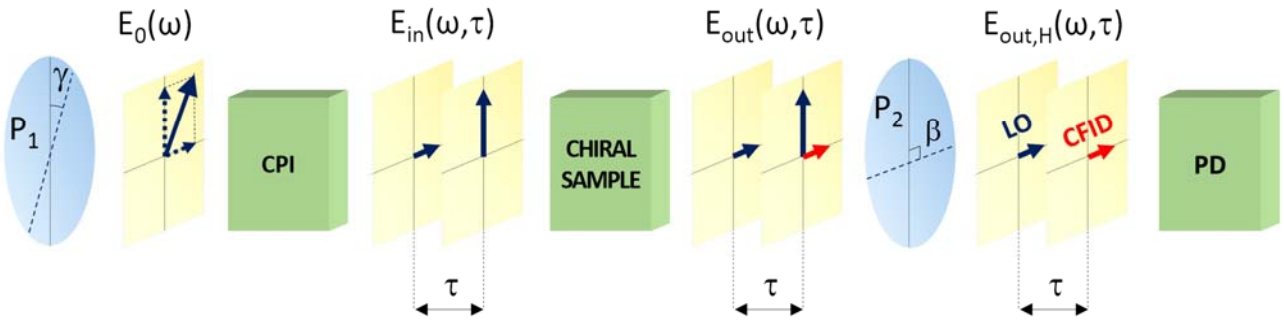

Figure 1. Conceptual scheme of the time-domain spectropolarimeter. A first polarizer P_1, oriented at a small angle γ with respect to the vertical, polarizes the light field $E_0(\omega)$ at the entrance of a common-path interferometer (CPI), which generates two replicas with perpendicular polarization, delayed by τ (field $E_{in}(\omega,\tau)$). The stronger vertical component interacts with the chiral sample, to generate a horizontal chiral field (CFID, red arrows), while the weaker horizontal component acts as a local oscillator (LO). If the second polarizer P_2 is oriented horizontally (β=90°), it selects the horizontal component $E_{out,H}(\omega,\tau)$ of the field emitted by the sample. The interference between the LO and the CFID (blue and red arrows) is read by a photodiode (PD) as a function of τ, generating an interferogram whose FT provides the CD/CB spectra.

where $\varphi=\omega\tau$ is the phase difference between H and V components introduced by the CPI, and τ is their relative delay. For an isotropic chiral sample with absorbance $\alpha=(\alpha_{LCP}+\alpha_{RCP})/2$, mean refractive index $n=(n_{LCP}+n_{RCP})/2$ and thickness L, the Jones matrix can be expressed, in the limit of weak CD and CB, as[20]:

$$M_{chiral} \approx 10^{-\alpha/2} e^{-i\rho} \begin{pmatrix} 1 & CB - iCD \\ -CB + iCD & 1 \end{pmatrix} \quad (2)$$

where $CB=(n_{LCP}-n_{RCP})L\omega/(2c)$ and $CD=(\alpha_{LCP}-\alpha_{RCP})\ln(10)/4$ are the optical rotation and ellipticity in radians, $\rho=nL\omega/c$ and c is the speed of light in vacuum. The electric field transmitted by the chiral sample is $E_{out}(\omega) = M_{chiral}\, E_{in}(\omega)$. After the sample, polarizer P_2 oriented along the H direction (β=90° in Fig. 1) selects the horizontal component of E_{out}:

$$E_{out,H}(\omega,\tau) = E_0(\omega) 10^{-\alpha/2} e^{-i\rho} \left[\sin\gamma + (CB - iCD)\cdot\cos\gamma\cdot e^{i\omega\tau}\right] \quad (3)$$

It consists of the superposition of the CFID field with the H component of E_{in} transmitted by the sample, which acts as a LO. By measuring with a single detector the intensity transmitted by polarizer P_2 as a function of the delay τ introduced by the CPI, and by integrating over all the monochromatic components, we obtain the chiral interferogram:

$$I_{chiral}(\tau) = \int d\omega \left|E_{out,H}(\omega,\tau)\right|^2 \cong \int d\omega \left|E_0(\omega)\right|^2 10^{-\alpha(\omega)} \cdot \left\{\sin^2\gamma + 2\sin\gamma\cos\gamma \cdot \left[CB(\omega)\cos(\omega\tau) - CD(\omega)\sin(\omega\tau)\right]\right\} \quad (4)$$

This expression contains the intensity of the LO and the mixing term between the LO and the CFID fields (self-heterodyne amplification), while the much weaker intensity of the CFID field has been neglected. By taking the imaginary and the real parts of the FT of the chiral interferogram $I_{chiral}(\tau)$, one can compute the CD and CB spectra, respectively. To obtain the absolute values of the signals, a calibration measurement must be performed with the second polarizer tilted by a well-defined angle β_{cal} (different from 0° or 90°), typically chosen at 45°. In this

case, the two replicas generated by the CPI interfere at the detector and the much weaker CFID can be neglected, yielding the calibration interferogram:

$$I_{cal}(\tau) = \int d\omega \left|E_0(\omega)\right|^2 10^{-\alpha(\omega)} \cdot \cdot \left\{ \left[1 - \cos(2\beta)\cos(2\gamma)\right]/2 + + \sin(2\beta) \cdot \sin\gamma \cdot \cos\gamma \cdot \cos(\omega\tau) \right\} \quad (5)$$

When taking the ratio of the FTs of the chiral and calibration interferograms, the light intensity $|E_0|^2$, sample absorbance and dependence on the polarizer angle γ cancel and we obtain:

$$CD(\omega) = -\frac{1}{2}\mathrm{Im}\left\{\frac{FT\left[I_{chiral}(\tau)\right]}{FT\left[I_{cal}(\tau)\right]}\right\}\sin 2\beta \quad (6)$$

$$CB(\omega) = \frac{1}{2}\mathrm{Re}\left\{\frac{FT\left[I_{chiral}(\tau)\right]}{FT\left[I_{cal}(\tau)\right]}\right\}\sin 2\beta \quad (7)$$

These equations remain valid even if the absolute value of τ is not known in the experiment (i.e. the position of the CPI corresponding to the zero optical path difference is not identified precisely). In such a case, the FT of $I_{cal}(\tau)$ can have an imaginary component. The division thus also replaces the (frequency-dependent) phase calibration that is necessary in conventional FT-VCD spectroscopy.

It may be noted that equations 6 and 7 are very similar to the equations needed to retrieve the CD and CB signals in the spectral interferometry approach of Rhee et al.[13] (see introduction). The main difference resides in the fact that our time-domain method directly computes the complex OA spectrum from the FTs of the chiral and calibration temporal interferograms, while the frequency-domain method measures spectral interferograms as non-complex signals. Therefore, a Kramers-Kroning transform, consisting in an inverse FT to the time domain, temporal filtering and FT back to the frequency domain, is needed to reconstruct the corresponding complex functions.

Equation (4) shows that the chiral interferogram $I_{chiral}(\tau)$ sits on an offset proportional to $\sin^2(\gamma)$, while the amplitude of the fringe pattern is proportional to $\sin(\gamma)\cdot\cos(\gamma)$, so that the modulation depth for the CD and CB signals is proportional to $\cot\gamma$. Therefore, small values of γ result in higher contrast of the fringes but reduce the amplitude of the fringe pattern, because the lower amplitude of the LO decreases the self-heterodyne amplification. In practice, the optimal choice of the polarizer angle γ depends on the amount of light available, the dynamic range of the detector and the quality of the polarizers. Typical values of γ range between 0.5 and 5°, thus achieving an amplification of the modulation depth by 1-2 orders of magnitude with respect to the symmetric case (γ=45°) and increasing the signal-to-noise ratio considerably. Largest amplification is possible with intense light sources like lasers, and this measurement principle has been used previously to significantly enhance CD (and CB) signals in frequency-domain measurements with wavelength selection both before[7,21] and after[22,23] the light passes the sample. On the other hand, if only CD signals are measured, the second polarizer (P_2 in Fig. 1) may be omitted in full analogy to the VCD setup in ref.[12], but with the much higher delay stability and reproducibility that allows us to extend the method to the UV-visible range. In this case, the H and V components of CPI output should be of equal strength (γ=45°), and the modulation depth of the chiral interferogram cannot be amplified. This may nevertheless be useful in some cases, because with polarizer P2 background signals due to residual linear dichroism and birefringence of the sample cell are equally

enhanced, and can only be suppressed by careful alignment.

Experimental setup

Figure 2 shows the experimental setup of our time-domain spectropolarimeter. It starts with a broadband light source, which can be either coherent or incoherent. For coherent excitation, we used a high-power supercontinuum fiber laser (NKT Photonics model SuperK Extreme EXW-12), emitting an ultra-broadband spectrum in the 500–2300 nm range with a power density higher than 2 mW/nm in the 550-1000 nm spectral region. As incoherent light source, we employed an off-the-shelf halogen lamp, emitting 310 lumens. The broadband illumination is sent to a first polarizer P1 (GTH5M-B, Thorlabs, extinction ratio $>10^5$), with transmission axis tilted from the vertical direction by a small angle γ. The light transmitted by the polarizer can be described as a superposition of an intense V polarized component and a weak H polarized component.

After the polarizer, the light passes the birefringent CPI, which is a simplified version of the Translating-Wedge-based Identical pulses eNcoding System (TWINS) system, previously introduced by some of the authors[24,25]. TWINS is composed of two blocks of a birefringent material, A and B, with optical axes (see blue arrow and dots in Fig. 2) rotated by 90° with respect to each other and perpendicular to the propagation direction of the beam. Block A is a parallel faces plate with V optical axis, which introduces a fixed delay between the V and H replicas. Block B is shaped in form of two identical wedges, with H optical axis, which introduce a delay of opposite sign. Accurate alignment of the optical axes of the birefringent elements is necessary in order to avoid spurious birefringence and is achieved by mounting them on goniometric stages. One of the wedges of block B is mounted on a precision translation stage (LMS-60 25 LM, Physik Instrumente), which allows changing its insertion and fine tuning of the overall thickness of block B. Note that, to minimize lateral displacement of the beam, the direction of motion is not exactly perpendicular to the light beam, but inclined by the apex angle of the wedge (see black thick double-sided arrow in Fig. 2). Therefore, as a function of the insertion of the moving wedge, the CPI introduces a variable delay τ between the V and H components with very high precision and long-term stability (on the order of a few attoseconds). For our experiments, we used α-barium borate as birefringent material. The thickness of the first block was 5 mm and we chose for the second block wedges with apex angle 9° and lateral dimension 25 mm, resulting in a maximum value for the delay $\tau_{max} = 1.5$ ps corresponding to a spectral resolution $\Delta\lambda = 0.8$ nm at 600 nm. One should note that TWINS works in a partially rotating frame[26], as it introduces, for a given wedges insertion, a frequency-dependent delay. For this reason, it is necessary

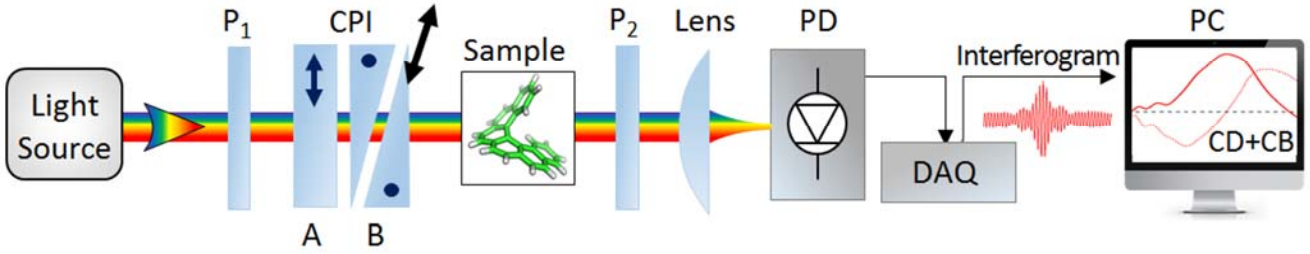

Figure 2. Experimental setup for the time-domain spectropolarimeter. P_1 and P_2: linear polarizers; CPI: common-path interferometer; PD: photodiode; DAQ: data acquisition card; PC, personal computer. Blue arrow and dots on the CPI indicate the direction of the optical axis, while black arrow indicates the direction of translation of the moving wedge x.

to perform a wavelength calibration of the setup, as described in the results section.

After the CPI, the two components pass the chiral sample and to second polarizer P_2 (identical to P_1) with transmission axis rotated by an angle β with respect to the vertical direction. The light transmitted by P_2 impinges on a photodiode (PDA20CS-EC, Thorlabs) connected to a data acquisition card and a computer. Upon scanning the TWINS delay with two different orientations of polarizer P2, the chiral (for $\beta = 90°$) and calibration (for $\beta = 45°$) interferograms are recorded and the CB and CD spectra are calculated according to Eqs (6) and (7).

RESULTS AND DISCUSSION

To test the performances of our time-domain spectropolarimeter, we have performed measurements on the two enantiomers of Nickel Tartrate dissolved in distilled water at a concentration of 120 mM. Figure 3(a) shows as a green line the calibration interferogram $I_{cal}(x)$ as a function of the wedge insertion x for an angle $\beta_{cal}=45°$. The FT of $I_{cal}(x)$ yields $I_{cal}(f_x)$, where f_x is a spatial frequency, which becomes the spectrum of the light transmitted by the sample $I_{cal}(\omega)$, shown as a green area in the top panel of Fig. 3(b), after calibration of the frequency axis using a set of narrowband interference filters (see Ref.[25] for a detailed description of the procedure). One can recognize the dip at 1150 nm, which corresponds to the absorption peak due to a d-d transitions of the complex. The chiral interferograms $I_{chiral}(x)$ for the (S,S) and (R,R) forms of Nickel Tartrate are shown in Fig. 3(a) as blue and red curves, respectively. By looking at the zooms around time zero in the inset, one can notice that: (i) the two interferograms are perfectly out of phase, and (ii) they are shifted with respect to the zero optical-path difference by the same quantity (approx. 1.5 optical cycles), because unlike $I_{cal}(\tau)$, $I_{chiral}(\tau)$ is not a symmetric function with respect to τ (see Eq. (4)). Figure 3(b) displays, as solid(dashed) lines, the CD(CB) spectra of both enantiomers (blue for the (S,S) form and red for the (R,R)

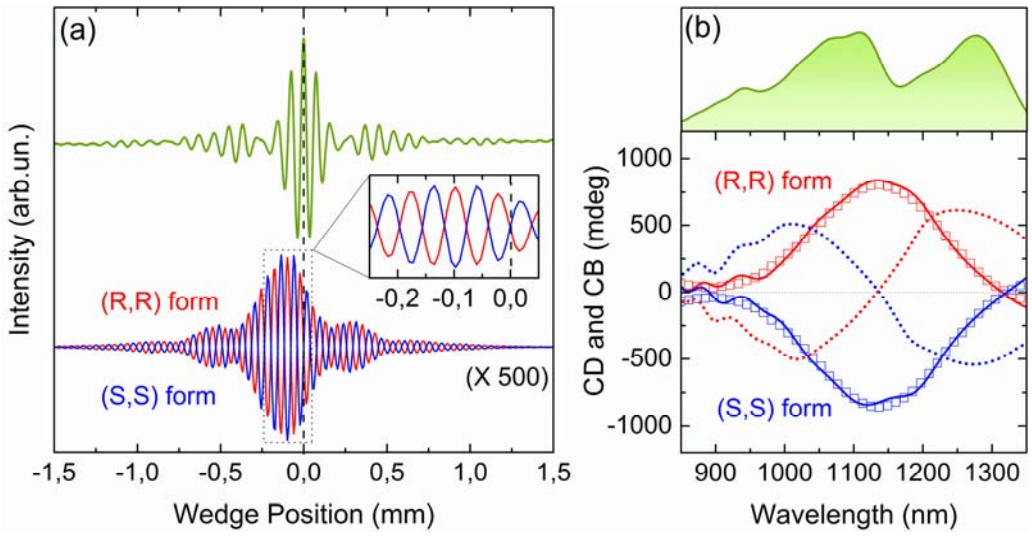

Figure 3. (a) Calibration interferogram, measured with $\beta = 45°$, for the excitation light transmitted by the sample (green curve) and chiral interferograms, measured with $\gamma = 4°$, of the two enantiomers of Nickel Tartrate (blue and red curves). The measurements were performed with a 310-lumen halogen lamp and the chiral interferograms was measured in 5 seconds and averaged 10 times. (b) Top panel: spectrum of the excitation light transmitted by the sample; bottom panel: CD and CB spectra (solid and dotted lines, respectively) of (R,R)-form (red curves) and (S,S)-form (blues curves) enantiomers of Nickel Tartrate. Red and blue circles are the CD spectra measured with a dispersive spectropolarimeter.

form) obtained from the imaginary(real) part of the FTs of the chiral interferograms. The CD signals measured with our time-domain spectropolarimeter display an excellent agreement, both in shape and in absolute value, with the signals measured by a standard dispersive spectropolarimeter[27], shown in Fig. 3(b) as red and blue squares for the (R,R) and (S,S) forms, respectively.

To demonstrate the capability of our instrument to accept ultra-broadband pulses, making it suitable for time-resolved measurements of optical activity on the femtosecond timescale, we have replaced the incoherent lamp with the broadband laser supercontinuum. The resulting CD signals for different tartrate concentrations are plotted in Fig. 4(a), showing a good reproducibility of the shape also for low concentrations, as reflected by the constant zero crossing at $\approx$1320 nm. Figure 4(b) shows the CD amplitude at λ=1135 nm as a function of concentration together with a linear fit, displaying the expected scaling of the signal with concentration. These measurements illustrate the quantitative capabilities of our time-domain spectropolarimeter, which are remarkable considering the simplicity of the experimental apparatus.

Our set-up combines two measurement principles of OA, polarization-division interferometry pioneered in the mid-IR for recording VCD spectra, and the use of crossed polarizers, which is the basis of traditional optical rotation (or CB) measurements. A PDI delay change of half an optical cycle inverts the handedness of the output light and delay scanning thereby eliminates the need of external polarization modulation. The frequency of polarization modulation is directly proportional to the scanning speed, which hence determines the signal-to-noise ratio of the measurement. With our CPI and standard translation stages, moving at a speed up to 100 mm/s, it is possible to reach the multiple-kHz modulation regime of PEMs, in particular in the UV-visible spectral range. At the same time, the birefringent wedges ensure a very high degree of perpendicular polarization of the two beam replicas, which minimizes any residual interference in the absence of a chiral sample. The common-path birefringent PDI can be readily extended to the mid-IR, using Hg2Cl2 (calomel) as birefringent material, as recently demonstrated[28]. It should thus not only be much simpler and cheaper, but also more sensitive than the Michelson-type PDIs in the mid-IR, which have so far not been developed into commercial devices.

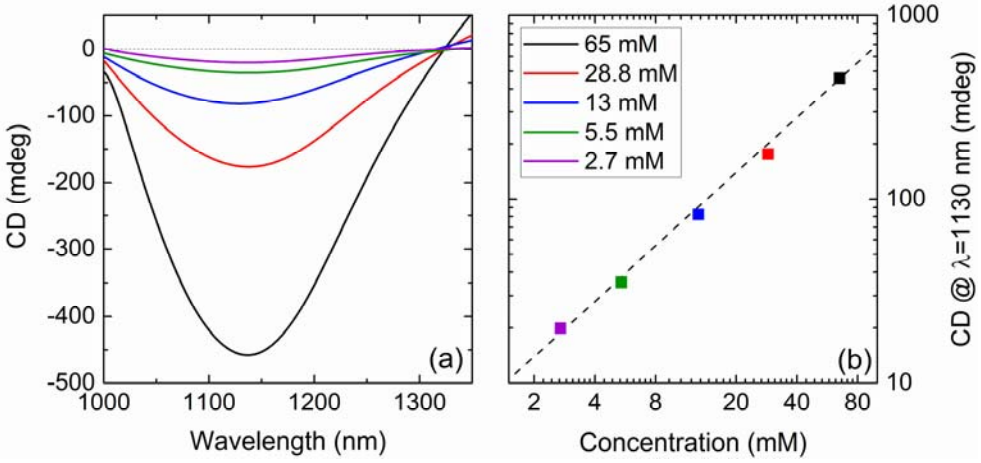

Figure 4. (a) CD spectra for the (S,S)-form of Nickel Tartrate at different concentrations, measured with a laser supercontinuum. (b) CD signal of Nickel Tartrate peak at λ = 1130 nm as a function of concentration (colored squares), together with a linear fit (dotted line).

CONCLUSIONS AND OUTLOOK

In this paper, we have introduced a novel approach to the broadband measurement of molecular optical activity, combining time-domain detection with heterodyne amplification. Our method relies on a birefringent common-path polarization-division interferometer, which creates two replicas of the input light with highly pure perpendicular polarizations and attosecond-level stability of their relative delay. The more intense replica interacting with the sample produces a chiral free-induction decay field, which is amplified by the other replica, acting as a phase-coherent local oscillator with user-selectable amplitude. The exceptional precision of our common-path interferometer allows us to record highly accurate interferograms without the need of active delay stabilization or tracking and to retrieve the CD and CB spectra using a single-pixel detector. Our device has a small footprint and reduced cost with respect to conventional spectropolarimeters, as it does not require a monochromator, a photo-elastic modulator nor a lock-in amplifier.

Our time-domain approach has great potential for time-resolved OA measurements to study ultrafast stereochemistry on the femtosecond - picosecond timescale[29], such as isomerization, ring opening, and structural rearrangements in light-driven unidirectional rotary motors[30,31]. The device can accept broadband ultrashort pulses with duration down to a few optical cycles, whereas standard spectropolarimeters in the UV-visible only allow for a monochromatic beam at the sample. Until now the beam-path of standard CD spectrometers had to be inverted for ultrafast transient OA measurements in the frequency domain, and light was dispersed behind the sample[22,32,33]. This makes the OA measurements very sensitive to artefacts caused by the highly polarization-sensitive optics of a spectrometer. While the read out rate of array detectors is limited to the kHz regime, time-domain detection makes it possible to modulate an actinic pump-pulse at much higher repetition rates, as already demonstrated in refs [34,35]. Demodulation of the collected signal as a function of pump-probe delay T and PDI delay τ with a lock-in amplifier should allow one to record the pump-induced differential chiral interferogram $\Delta I_{\mathrm{chiral}}(\tau,T)$ with very high signal-to-noise, from which the transient differential OA spectra $\Delta CD(\omega,T)$ and $\Delta CB(\omega,T)$ can be obtained by FT.

ACKNOWLEDGMENTS

This work was supported by the European Research Council under the Proof of Concept Grant CHIMERA (ERC-2016-PoC No. 754802), the Consolidator Grant VIBRA (ERC-2014-CoG No. 648615), the Advanced Grant STRATUS (ERC-2011-AdG No. 291198), the Proof of Concept Grant MISSION (ERC-2014-POC No. 665635) and by the Swiss National Science Foundation (SNF) (No. 200020_143487). We would like to gratefully acknowledge fruitful discussions and experimental help from Prof. Sergio Abbate, Prof. Giovanna Longhi, Dr. Giuseppe Mazzeo and Dr. Ettore Castiglioni.

REFERENCES

1 Berova N, Polavarapu PL, Nakanishi K, Woody RW (eds.). *Comprehensive Chiroptical Spectroscopy, Volume 2, Applications in Stereochemical Analysis of Synthetic Compounds, Natural Products, and Biomolecules*. Wiley, 2012.

2 Barron LD. *Molecular Light Scattering and Optical Activity*. Cambridge University Press: Cambridge, 2004.

3 Berova N, Nakanishi K, Woody RW (eds.). *Circular Dichroism: Principles and Applications, 2nd Edition*. Wiley - VCH, 2000.

4 Sreerama N, Woody RW. Computation and Analysis of Protein Circular Dichroism Spectra. *Methods Enzymol* 2004; **383**: 318–351.

5 Fasman GD (ed.). *Circular Dichroism and the Conformational Analysis of Biomolecules*. Springer US: Boston, MA, 1996.

6 Hentschel M, Schäferling M, Duan X, Giessen H, Liu N. Chiral plasmonics. *Sci Adv* 2017; **3**: 1–13.

7 Helbing J, Bonmarin M. Vibrational circular dichroism signal enhancement using self-heterodyning with elliptically polarized laser pulses. *J Chem Phys* 2009; **131**: 174507.

8 Rhee H, Eom I, Ahn S-H, Cho M. Coherent electric field characterization of molecular chirality in the time domain. *Chem Soc Rev* 2012; **41**: 4457–4466.

9 Lombardi RA, Nafie LA. Observation and calculation of vibrational circular birefringence: A new form of vibrational optical activity. *Chirality* 2009; **21**: E277–E286.

10 Polavarapu PL (ed.). *Principles and Applications of Polarization-Division Interferometry*. Wiley - VCH, 1997.

11 Ragunathan N, Lee NS, Freedman TB, Nafie LA, Tripp C, Buijs H. Measurement of vibrational circular dichroism using a polarizing Michelson interferometer. *Appl Spectrosc* 1990; **44**: 5–7.

12 Polavarapu PL, Deng Z, Chen G-C. Polarization-Division Interferometry: Time-Resolved Infrared Vibrational Dichroism Spectroscopy. *Appl Spectrosc* 1995; **49**: 229–236.

13 Rhee H, June Y-G, Lee J-S, Lee K-K, Ha J-H, Kim ZH *et al.* Femtosecond characterization of vibrational optical activity of chiral molecules. *Nature* 2009; **458**: 310–313.

14 Rhee H, Choi J, Cho M. Infrared Optical Activity: Electric Field Approaches in Time Domain. *Acc Chem Res* 2010; **43**: 1527–1536.

15 Lepetit L, Chériaux G, Joffre M. Linear techniques of phase measurement by femtosecond spectral interferometry for applications in spectroscopy. *J Opt Soc Am B* 1995; **12**: 2467–2474.

16 Rhee H, Ha J-H, Jeon S-J, Cho M. Femtosecond spectral interferometry of optical activity: Theory. *J Chem Phys* 2008; **129**: 94507.

17 Eom I, Ahn S-H, Rhee H, Cho M. Single-Shot Electronic Optical Activity Interferometry: Power and Phase Fluctuation-Free Measurement. *Phys Rev Lett* 2012; **108**: 103901.

18 Hiramatsu K, Nagata T. Communication: Broadband and ultrasensitive femtosecond time-resolved circular dichroism spectroscopy. *J Chem Phys* 2015; **143**: 121102.

19 Jones RC. A New Calculus for the Treatment of Optical SystemsI Description and Discussion of the Calculus. *J Opt Soc Am* 1941; **31**: 488–493.

20 Xie X, Simon JD. Picosecond circular dichroism spectroscopy: a Jones matrix analysis. *J Opt Soc Am B* 1990; **7**: 1673–1684.

21 Niezborala C, Hache F. Measuring the dynamics of circular dichroism in a pump-probe experiment with a Babinet-Soleil compensator: erratum. *J Opt Soc Am B* 2006; **23**: 2418–2424.

22 Dutta B, Helbing J. Optimized interferometric setup for chiral and achiral ultrafast IR spectroscopy. *Opt Express* 2015; **23**: 16449–16465.

23 Eom I, Ahn S-H, Rhee H, Cho M. Broadband near UV to visible optical activity measurement using self-heterodyned method. *Opt Express* 2011; **19**: 10017–10028.

24 Brida D, Manzoni C, Cerullo G. Phase-locked pulses for two-dimensional spectroscopy by a birefringent delay line. *Opt Lett* 2012; **37**: 3027–3029.

25 Preda F, Oriana A, Réhault J, Lombardi L, Ferrari AC, Cerullo G *et al.* Linear and Nonlinear Spectroscopy by a Common-Path Birefringent Interferometer. *IEEE J Sel Top Quantum Electron* 2017; **23**: 88–96.

26 Réhault J, Maiuri M, Oriana A, Cerullo G. Two-dimensional electronic spectroscopy with birefringent wedges. *Rev Sci Instrum* 2014; **85**: 123107.

27 Castiglioni E, Lebon F, Longhi G, Abbate S. Vibrational Circular Dichroism in the Near Infrared: Instrumental Developments and Applications. *Enantiomer A J Sterochemistry* 2002; **7**: 161–173.

28 Réhault J, Borrego-Varillas R, Oriana A, Manzoni C, Hauri CP, Helbing J *et al.* Fourier transform spectroscopy in the vibrational fingerprint region with a birefringent interferometer. *Opt Express* 2017; **25**: 4403–4412.

29 Meyer-Ilse J, Akimov D, Dietzek B. Recent advances in ultrafast time-resolved chirality measurements: Perspective and outlook. *Laser Photonics Rev* 2013;

7: 495–505.

30 Strambi A, Durbeej B, Ferré N, Olivucci M. Anabaena sensory rhodopsin is a light-driven unidirectional rotor. *Proc Natl Acad Sci U S A* 2010; **107**: 21322–21326.

31 Conyard J, Addison K, Heisler I a., Cnossen A, Browne WR, Feringa BL *et al.* Ultrafast dynamics in the power stroke of a molecular rotary motor. *Nat Chem* 2012; **4**: 547–551.

32 Trifonov A, Buchvarov I, Lohr A, Würthner F, Fiebig T. Broadband femtosecond circular dichroism spectrometer with white-light polarization control. *Rev Sci Instrum* 2010; **81**: 43104.

33 Mangot L, Taupier G, Romeo M, Boeglin A, Cregut O, (Honorat) Dorkenoo KD. Broadband transient dichroism spectroscopy in chiral molecules. *Opt Lett* 2010; **35**: 381–383.

34 Réhault J, Crisafi F, Kumar V, Ciardi G, Marangoni M, Cerullo G *et al.* Broadband stimulated Raman scattering with Fourier-transform detection. *Opt Express* 2015; **23**: 25235–25246.

35 Preda F, Kumar V, Crisafi F, Figueroa del Valle DG, Cerullo G, Polli D. Broadband pump-probe spectroscopy at 20-MHz modulation frequency. *Opt Lett* 2016; **41**: 2970–2973.

List of Figure Captions

Figure 1. Conceptual scheme of the time-domain spectropolarimeter. A first polarizer P_1, oriented at a small angle γ with respect to the vertical, polarizes the light field $E_0(\omega)$ at the entrance of a common-path interferometer (CPI), which generates two replicas with perpendicular polarization, delayed by τ (field $E_{in}(\omega,\tau)$). The stronger vertical component interacts with the chiral sample, to generate a horizontal chiral field (CFID, red arrows), while the weaker horizontal component acts as a local oscillator (LO). If the second polarizer P_2 is oriented horizontally (β=90°), it selects the horizontal component $E_{out,H}(\omega,\tau)$ of the field emitted by the sample. The interference between the LO and the CFID (blue and red arrows) is read by a photodiode (PD) as a function of τ, generating an interferogram whose FT provides the CD/CB spectra.

Figure 2. Experimental setup for the time-domain spectropolarimeter. P_1 and P_2: linear polarizers; CPI: common-path interferometer; PD: photodiode; DAQ: data acquisition card; PC, personal computer. Blue arrow and dots on the CPI indicate the direction of the optical axis, while black arrow indicates the direction of translation of the moving wedge x.

Figure 3. (a) Calibration interferogram, measured with $\beta = 45°$, for the excitation light transmitted by the sample (green curve) and chiral interferograms, measured with $\gamma = 4°$, of the two enantiomers of Nickel Tartrate (blue and red curves). The measurements were performed with a 310-lumen halogen lamp and the chiral interferograms was measured in 5 seconds and averaged 10 times. (b) Top panel: spectrum of the excitation light transmitted by the sample; bottom panel: CD and CB spectra (solid and dotted lines, respectively) of (R,R)-form (red curves) and (S,S)-form (blues curves) enantiomers of Nickel Tartrate. Red and blue circles are the CD spectra measured with a dispersive spectropolarimeter.

Figure 4. (a) CD spectra for the (S,S)-form of Nickel Tartrate at different concentrations, measured with a laser supercontinuum. (b) CD signal of Nickel Tartrate peak at $\lambda = 1130$ nm as a function of concentration (colored squares), together with a linear fit (dotted line).

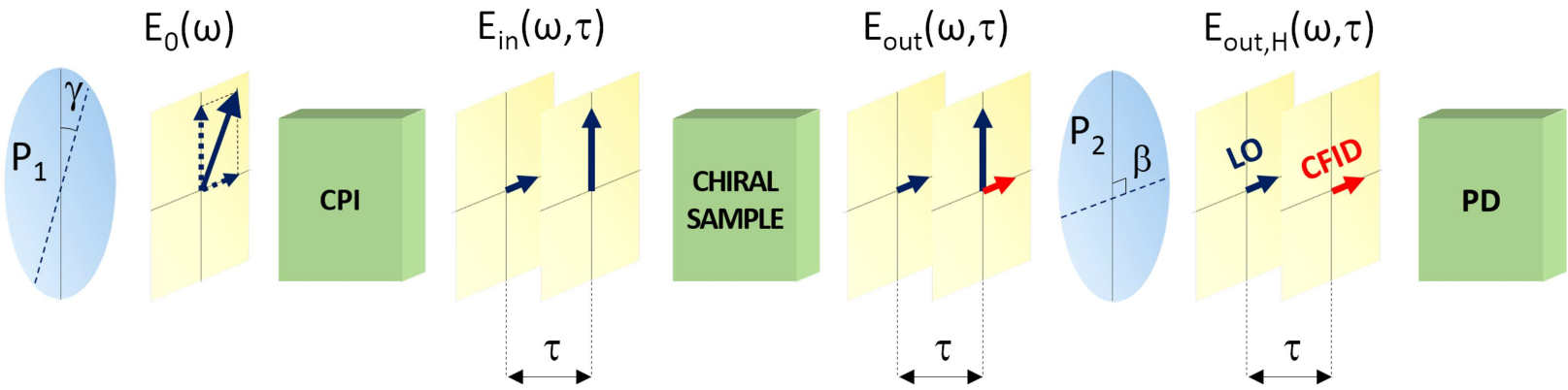
$E_0(\omega)$
$E_{in}(\omega,\tau)$
$E_{out}(\omega,\tau)$
$E_{out,H}(\omega,\tau)$
P_1
γ
CPI
CHIRAL SAMPLE
P_2
β
LO
CFID
PD
τ
τ
τ

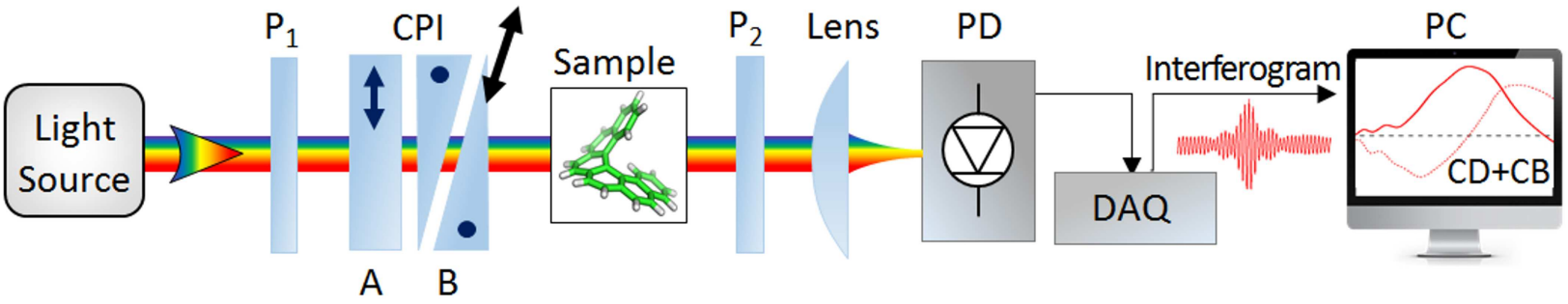
Light Source
P1
CPI
A
B
Sample
P2
Lens
PD
DAQ
Interferogram
PC
CD+CB

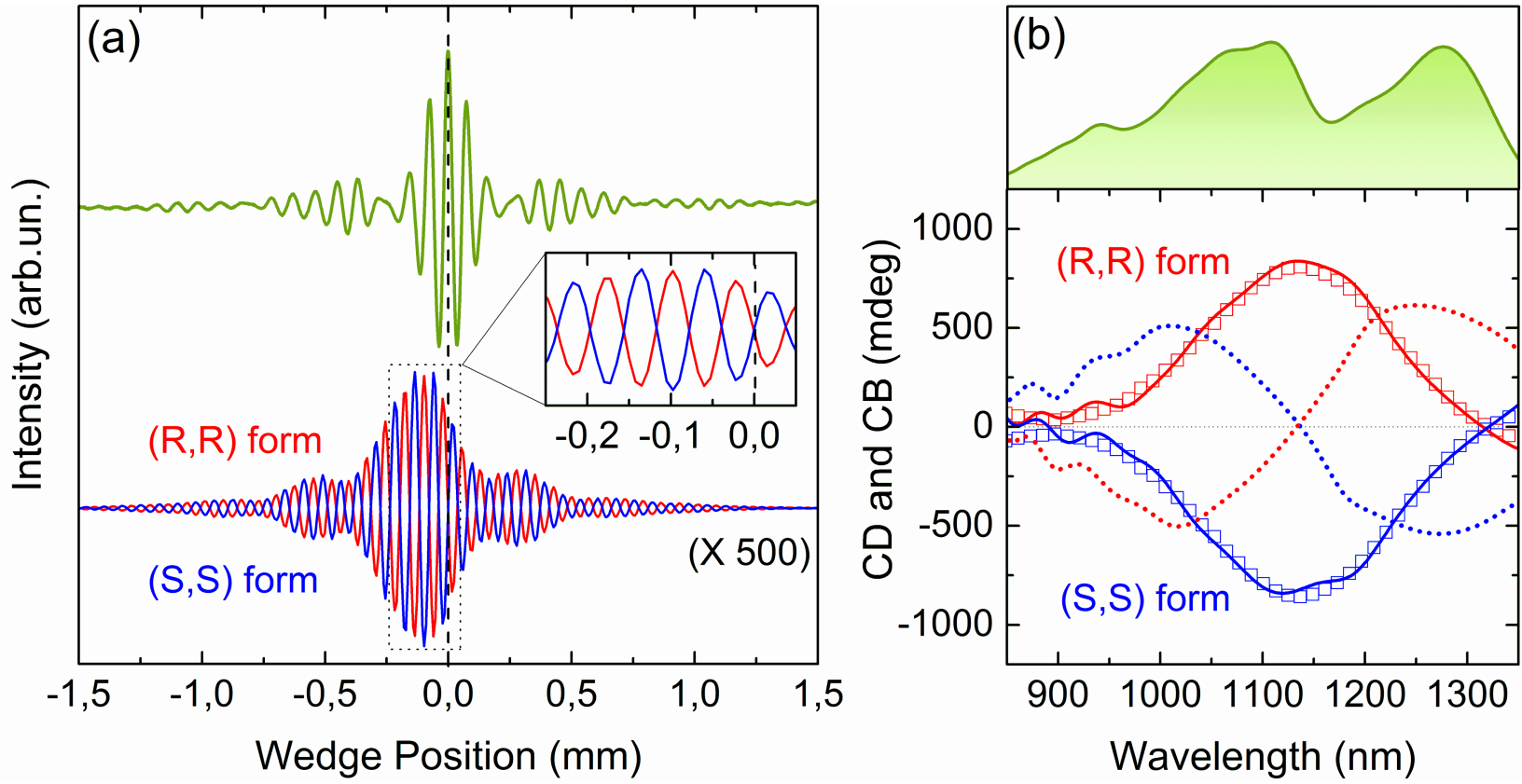
(a)
Intensity (arb.un.)
(R,R) form
(S,S) form
(X 500)
-0,2 -0,1 0,0
-1,5 -1,0 -0,5 0,0 0,5 1,0 1,5
Wedge Position (mm)
(b)
CD and CB (mdeg)
1000
500
0
-500
-1000
(R,R) form
(S,S) form
900 1000 1100 1200 1300
Wavelength (nm)

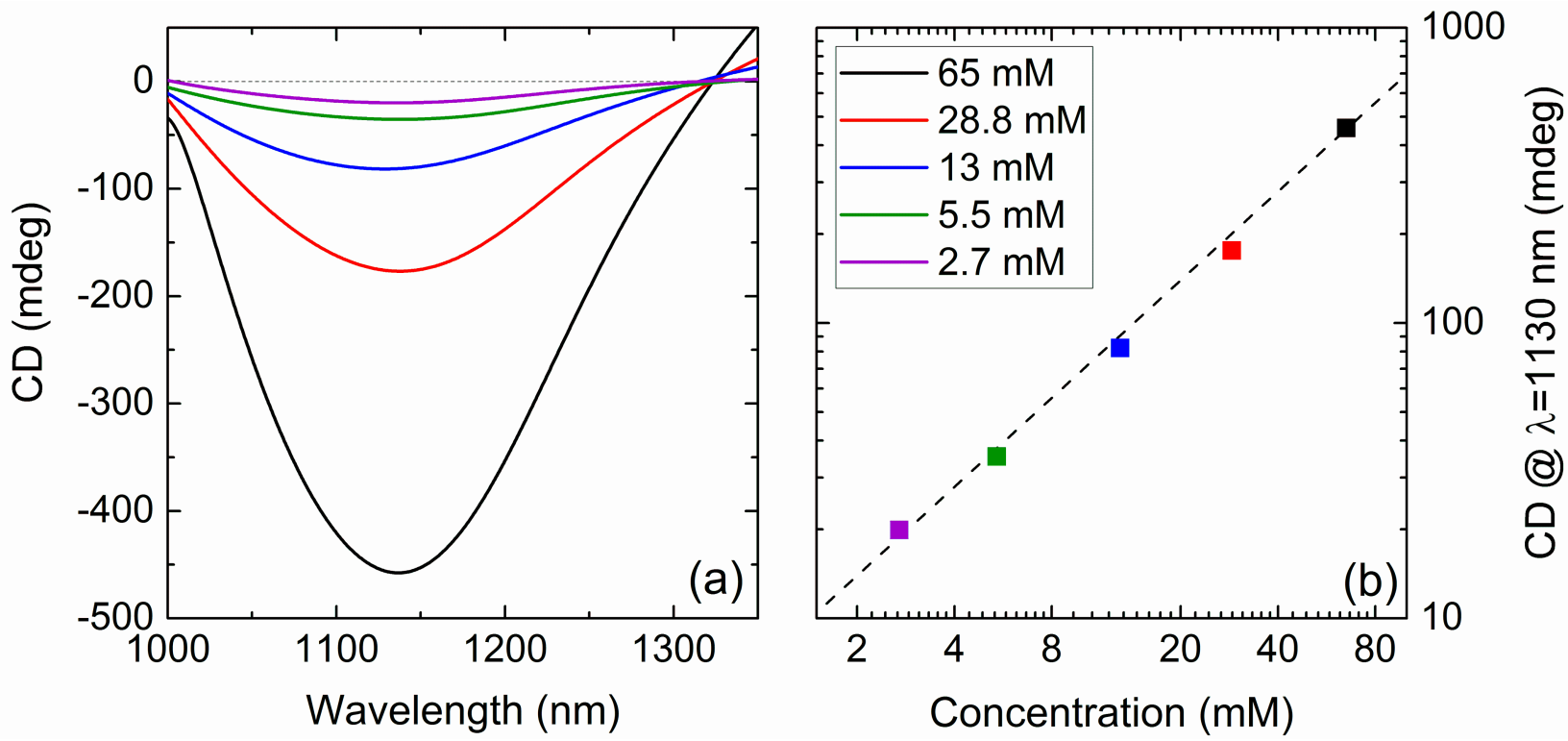
0
-100
-200
-300
-400
-500
CD (mdeg)
1000
1100
1200
1300
Wavelength (nm)
(a)
65 mM
28.8 mM
13 mM
5.5 mM
2.7 mM
2
4
8
20
40
80
Concentration (mM)
(b)
1000
100
10
CD @ λ=1130 nm (mdeg)